Monthly Notices
of the
ROYAL ASTRONOMICAL SOCIETY

MNRAS **452,** 3293–3303 (2015) doi:10.1093/mnras/stv1569

GRB host galaxies with VLT/X-Shooter: properties at $0.8 < z < 1.3$

S. Piranomonte,[1]★ J. Japelj,[2] S. D. Vergani,[3,4] S. Savaglio,[5,6,7] E. Palazzi,[8] S. Covino,[4] H. Flores,[3] P. Goldoni,[9] G. Cupani,[10] T. Krühler,[11,12] F. Mannucci,[13] F. Onori,[14] A. Rossi,[8] V. D'Elia,[1,15] E. Pian,[8,16] P. D'Avanzo,[4] A. Gomboc,[2] F. Hammer,[3] S. Randich,[13] F. Fiore,[1] L. Stella[1] and G. Tagliaferri[4]

[1]*INAF-Osservatorio Astronomico di Roma, via Frascati 33, I-00040 Monte Porzio Catone (RM), Italy*
[2]*Faculty of Mathematics and Physics, University of Ljubljana, Jadranska ulica 19, SI-1000 Ljubljana, Slovenia*
[3]*Laboratoire Galaxies Etoiles Physique et Instrumentation, Observatoire de Paris, 5 place Jules Janssen, F-92195 Meudon, France*
[4]*INAF-Osservatorio Astronomico di Brera, via E. Bianchi 46, I-23807 Merate (LC), Italy*
[5]*Physics Department, University of Calabria, via P. Bucci, I-87036 Arcavacata di Rende, Italy*
[6]*European Southern Observatory, Karl-Schwarzschild-Strasse 2, D-85748 Garching bei Munchen, Germany*
[7]*Max Planck Institute for Extraterrestrial Physics, D-85748 Garching bei Munchen, Germany*
[8]*INAF-Istituto di Astrofisica Spaziale e Fisica Cosmica, Sezione di Bologna, via Gobetti 101, I-40129 Bologna, Italy*
[9]*APC, Univ. Paris Diderot, CNRS/IN2P3, CEA/Irfu, Obs. de Paris, Sorbonne, F-75205 Paris Cité, France*
[10]*INAF-Osservatorio Astronomico di Trieste, via G.B. Tiepolo 11, I-34143 Trieste, Italy*
[11]*European Southern Observatory, Alonso de Cordova 3107, Vitacura, Casilla 19001, Santiago 19, Chile*
[12]*Dark Cosmology Centre, Niels Bohr Institute, University of Copenhagen, Juliane Maries Vej 30, DK-2100 Kobenhavn 0, Denmark*
[13]*INAF-Osservatorio Astrofisico di Arcetri, INAF, Largo E. Fermi 5, F-50125 Firenze, Italy*
[14]*Dipartimento di Matematica e Fisica, Universitá degli Studi Roma Tre, Via della Vasca Navale 84, I-00146 Roma, Italy*
[15]*ASI-Science Data Center, Via del Politecnico snc, I-00133 Rome, Italy*
[16]*Scuola Normale Superiore, Piazza dei Cavalieri 7, I-56126 Pisa, Italy*

Accepted 2015 July 10. Received 2015 June 15; in original form 2015 April 21

ABSTRACT

Long gamma-ray bursts (LGRBs) are associated with the death of massive stars. Their host galaxies therefore represent a unique class of objects tracing star formation across the observable Universe. Indeed, recently accumulated evidence shows that GRB hosts do not differ substantially from general population of galaxies at high ($z > 2$) redshifts. However, it has been long recognized that the properties of $z < 1.5$ hosts, compared to general star-forming population, are unusual. To better understand the reasons for the supposed difference in LGRB hosts properties at $z < 1.5$, we obtained Very Large Telescope (VLT)/X-Shooter spectra of six hosts lying in the redshift range of $0.8 < z < 1.3$. Some of these hosts have been observed before, yet we still lack well-constrained information on their characteristics such as metallicity, dust extinction and star formation rate (SFR). We search for emission lines in the VLT/X-Shooter spectra of the hosts and measure their fluxes. We perform a detailed analysis, estimating host average extinction, SFRs, metallicities and electron densities where possible. Measured quantities of our hosts are compared to a larger sample of previously observed GRB hosts at $z < 2$. SFRs and metallicities are measured for all the hosts analysed in this paper and metallicities are well determined for four hosts. The mass–metallicity relation, the fundamental metallicity relation and SFRs derived from our hosts occupy similar parameter space as other host galaxies investigated so far at the same redshift. We therefore conclude that GRB hosts in our sample support the found discrepancy between the properties of low-redshift GRB hosts and the general population of star-forming galaxies.

Key words: gamma-ray burst: general – galaxies: abundances – galaxies: distances and redshifts.

★ E-mail: silvia.piranomonte@oa-roma.inaf.it

© 2015 The Authors
Published by Oxford University Press on behalf of the Royal Astronomical Society

Downloaded from http://mnras.oxfordjournals.org/ at CNR on December 9, 2015

1 INTRODUCTION

Long duration gamma-ray bursts (LGRBs) originate from the deaths of very massive stars. This is supported both from observational (Galama et al. 1998; Hjorth & Bloom 2012) and theoretical (Paczyński 1998; MacFadyen & Woosley 1999; Woosley & Heger 2006) evidence. Thanks to their exceptional brightness they can be used as powerful sources to unveil the properties of their host galaxies at different epochs in the Universe. LGRB host galaxies form a unique sample of galaxies, covering a wide redshift range. First studies of LGRB hosts found them to be sub-luminous and blue (Le Floc'h et al. 2003), moderately star forming (SFR $\sim$1–10 $M_\odot$ yr^{-1}), with stellar masses of $\sim$1–5 $\times$ 10^9 $M_\odot$ and a high specific star formation rate (sSFR = SFR/M_*; Savaglio, Glazebrook & Le Borgne 2009). Later it was found that the hosts of the so-called dark GRBs (Jakobsson et al. 2004; van der Horst et al. 2009) are more dusty and massive (Perley et al. 2009, 2013; Hunt et al. 2014). GRB hosts are not selected according to their luminosity, but rather to the fact that a peculiar type of explosion of a massive star has occurred. Therefore, to first order, they trace regions of star formation at all epochs (Kistler, Yuksel & Hopkins 2013; Hunt et al. 2014).

LGRBs are associated with broad-lined type Ibc supernovae (e.g. Hjorth & Bloom 2012 and references therein; see however GRB 060614: Della Valle et al. 2006; Fynbo et al. 2006; Gal-Yam et al. 2006). It is still not clear which are the conditions that lead a massive star to have the special kind of core collapse that triggers the formation of a jet and an LGRB. Metallicity (which in single star progenitors is directly coupled with rotation) is one of the fundamental parameters predicted to impact the evolution of massive stars as well as their explosive deaths and is expected to play a fundamental role in the formation of LGRBs (e.g. Woosley 1993; MacFadyen & Woosley 1999; Heger et al. 2003; Yoon, Woosley & Langer 2010). Since theoretical models predict LGRBs occur preferentially in a low-metallicity environment, a special attention has been given to the study of chemical abundances in their hosts. While some studies did not find a statistically significant difference between these hosts and a general star-forming galaxy population (Savaglio et al. 2009), others found that LGRB hosts have substantially lower metallicities compared with the field galaxies at the same stellar mass (e.g. Levesque et al. 2010; Graham & Fruchter 2013). The observed preference for low metallicities could be a consequence of the occurrence of long GRBs in low-mass, actively star-forming galaxies, which dominate the current cosmic SFR (Mannucci et al. 2010; Mannucci, Salvaterra & Campisi 2011; Campisi et al. 2011; but see Graham & Fruchter 2013). Detections of LGRBs in high-metallicity environments suggest that not all LGRB hosts are necessarily characterized by low metallicity and that the metallicity threshold for a GRB production is not as low as predicted by theoretical models (Levesque et al. 2010; Elliott et al. 2013; Krühler et al. 2015; Perley et al. 2015c). Especially at low redshifts ($z < 1.5$), LGRB hosts also differ from other galaxies in properties like star formation rate (SFR) and stellar mass (Boissier et al. 2013; Perley et al. 2013; Vergani et al. 2014). To understand the reasons for biased hosts at $z < 1.5$, more observations of low-z hosts are necessary.

Most of the investigated samples of LGRB hosts are not carefully assembled due to small size or observational limitations. However, Vergani et al. (2014) used a sample which is nearly complete in redshift and unbiased against galaxies in which bright LGRBs exploded (Salvaterra et al. 2012; Melandri et al. 2012) and showed that $z < 1$ hosts tend to avoid massive galaxies and that this is likely linked to the metallicity of the host. This study showed that, in order to understand the host environment of LGRBs and the reason for the discrepancy between the field galaxies and the LGRB hosts, we should study different aspects of galaxies (e.g., stellar masses, SFRs and metallicities) simultaneously.

X-Shooter is a second generation instrument mounted at VLT/ESO (Vernet et al. 2011). It has a unique capability to produce intermediate resolution spectra ($R \sim$ 4000–17 000, depending on wavelength and slit width) while simultaneously covering a spectral range from 3000 to 24 000 Å. The instrument enables us to better characterize the LGRB host population and to explore galaxy formation and evolution beyond the parameter space provided by traditional high-z galaxy surveys.

In this paper, we present X-Shooter observations of six LGRB host galaxies that lie at $z \sim 1$. The observations were performed during our X-Shooter Guaranteed Time Observation (GTO) programme at the VLT/X-Shooter spectrograph.[1] Some of these hosts have been observed before but lack a good constraint on their metallicity, dust extinction and SFR and some of them have never been observed before. The aim of the survey, and presented study, was to detect emission lines of these LGRB host galaxies in order to measure the mentioned characteristics.

The sample, the observing program and the reduction of the X-Shooter data are presented in Section 2. The measurement procedure of galaxy characteristics is outlined in Section 3. A detailed account on results is given in Section 4 and we discuss them in Section 5. Summary and conclusions are shown in Section 6.

2 SAMPLE, OBSERVATIONS AND DATA REDUCTION

2.1 The sample

In this work, we present a study of six LGRB host galaxies observed during our GTO program. The hosts of GRB 000210 (Gorosabel et al. 2003a), GRB 000418 (Gorosabel et al. 2003b; Hatsukade et al. 2011), GRB 000911 (Price et al. 2002; Masetti et al. 2005), GRB 080413B, GRB 100316B and GRB 100724A, were selected because, due to their redshift (in the range $0.8 < z < 1.3$), they were either lacking the measured values of metallicity, dust extinction and SFR or these quantities were very poorly constrained. The spectral coverage and sensitivity of the X-Shooter allows us to get the whole set of lines ([O II], [O III], Hα, [N II]) necessary to perform these measurements. We started our observing program shortly after the end of the X-Shooter commissioning phase, hence three of the observed hosts (GRB 000210, GRB 000418 and GRB 000911) were selected also because they had previous spectroscopic observations with other telescopes and had one emission line detected (generally [O II]) in their spectrum. This would have allowed us to make a comparison of the X-Shooter results with the previous measurements and understand better the instrument performances. For the remaining three galaxies: the host of GRB 080413B was observed only in imaging, while the hosts of GRB 100316B and GRB 100724A were never observed before. The images we used to build finding charts of these last three hosts (Fig. 1), from which spectra we had a lower limit on the redshift, are dominated by afterglow emission. We are aware that this is a very small sample whose implications are discussed in Section 5.

[1] P.I.'s: H. Flores and S. Piranomonte from 2009 to 2012.

Downloaded from http://mnras.oxfordjournals.org/ at CNR on December 9, 2015

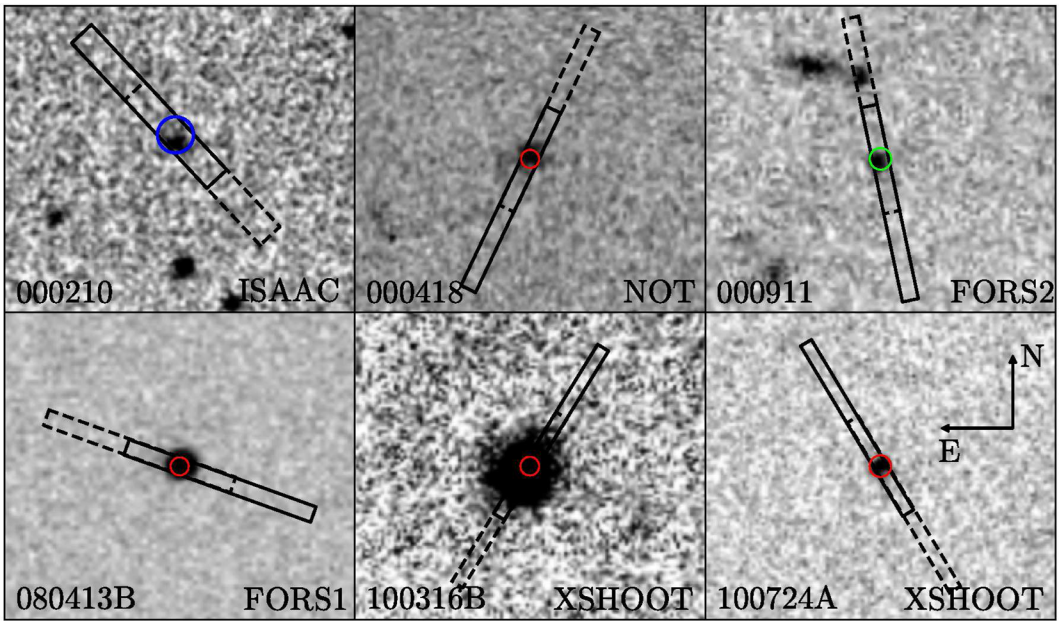

Figure 1. Mosaic of 17 arcsec × 17 arcsec regions centred on the positions of the six LGRBs as measured from the afterglow detection. Top three images were obtained several months after the LGRB detection and show the host galaxy. No late-time imaging has been performed for GRBs 100316B and 100724A and no image of the host of GRB 080413B is publicly available, therefore the bottom three images show the optical afterglow. Circles indicate the uncertainty of measured X-ray (blue), optical (red) and radio (green) afterglow positions. The placement of the (11 arcsec long) slit as well as the instrument with which the image was obtained are also indicated. All hosts were observed in nodding ABBA sequence with a 5 arcsec offset between A and B slit positions. A and B slit positions are plotted with full and dashed line, respectively.

2.1.1 GRB 000210 host

GRB 000210 was discovered by *BeppoSAX* (Piro et al. 2002). No optical afterglow was detected down to $R > 23.5$, leading to the classification of this burst as *dark* (e.g. Jakobsson et al. 2004). The field was observed by the X-ray *Chandra* telescope 21 h after the burst which led to the localization of the X-ray afterglow with an accuracy of 0.6 arcsec radius error circle (Piro et al. 2002, fig. 1). The *J*-band image of the host shown in Fig. 1 has been obtained with ISAAC at the VLT on 2001 September (Gorosabel et al. 2003a).

UV-NIR photometric observations were used to measure the stellar mass of $\approx 10^{9.3}$ $M_\odot$ (Savaglio et al. 2009; Svensson et al. 2010; Schady et al. 2014). Including a detection in the sub-mm band, Michałowski et al. (2008) found a value of $\sim 10^{10}$ $M_\odot$.

Previous spectral and UV–NIR photometric observations enabled the measurement of the host's SFR $\sim 2\,M_\odot$ yr^{-1} (Gorosabel et al. 2003a; Savaglio et al. 2009). A detection of sub-mm emission towards the position of GRB 000210 was interpreted as originating from the host galaxy and hence suggesting a SFR of several hundred $M_\odot$ yr^{-1} (Berger et al. 2003; Barnard et al. 2003; Michałowski et al. 2008).

2.1.2 GRB 000418 host

The optical afterglow of GRB 000418 was found to be very red with $R - K \approx 4$ (Vega-calibrated magnitudes; Klose et al. 2000), suggesting a very dusty sightline environment. A recent modelling of UV–NIR photometric spectral energy distribution (SED), assuming Calzetti et al. (2000) extinction curve, found an average host extinction of $A_V = 1.3$ mag (Perley et al. 2013; Schady et al. 2014). The *R*-band image of the host (Fig. 1) has been obtained with ALFOSC at the Nordic Optical Telescope approximately 1 yr after the burst (Gorosabel et al. 2003b).

UV–NIR photometric observations were used to measure the stellar mass of $M_* \approx 10^9$ $M_\odot$ (Savaglio et al. 2009; Svensson et al. 2010; Schady et al. 2014). Previous detection of the [O II] line enabled the measurement of the host's $\mathrm{SFR}_{[\mathrm{O\,II}]} = 55\,M_\odot \mathrm{yr}^{-1}$. The host was also detected in sub-millimetre and radio, suggesting higher values of SFR $\sim$ 250–900 $M_\odot$ yr^{-1} (Berger et al. 2003).

2.1.3 GRB 000911 host

Broad-band photometric SED modelling of the compact GRB 000911 host is consistent with a sub-luminous galaxy ($L < L_\star$), dominated by an old stellar population, and an average extinction $A_V = 0.3$–0.5, assuming a Large Magellanic Cloud (Fitzpatrick 1986) or starburst galaxy (Calzetti et al. 2000) extinction law (Masetti et al. 2005). The *I*-band image of the host in Fig. 1 has been obtained with FORS2 at the VLT approximately 1 yr after the burst (Masetti et al. 2005).

UV–NIR photometric observations were used to measure the stellar mass of $M_* \approx 10^{9.3}$ $M_\odot$ (Savaglio et al. 2009; Svensson et al. 2010). Previously detected [O II] enabled to calculate the $\mathrm{SFR}_{[\mathrm{O\,II}]} \approx 2.2\,M_\odot$ yr^{-1} (Price et al. 2002; Savaglio et al. 2009).

2.1.4 GRB 080413B host

To measure the stellar mass of the host of GRB 080413B, we use the host observations from GROND (Filgas et al. 2011) as well as public *Spitzer*/IRAC data taken as part of the SHOALS survey (Perley et al. 2015a,c). IRAC magnitudes were determined based on PBCD data from the archive, circular apertures and tabulated zero-points. No other galaxies are detected within the immediate vicinity of the host of GRB 080413B, and a possible confusion in the IRAC data is no concern in our analysis.

Downloaded from http://mnras.oxfordjournals.org/ at CNR on December 9, 2015

Table 1. Presentation of the sample and observation log. In columns 1 to 10 we report the GRB name, its host galaxy redshift (measured from emission lines detected in our X-shooter spectra, see Section 4), Galactic colour excess, the date of observation together with the observing run, seeing condition, binning, spectrograph arm, total exposure time, slit width and wavelength resolution at the centre of each arm, respectively. All observations were performed in NODDING mode. We report the average seeing measured by ESO-DIMM (Sarazin & Roddier 1990) at the time of observations.

LGRB host	Redshift	E(B−V)	Date Programme ID	Seeing	Binning	Arm	Exp. Time (s)	Slit width (arcsec)	Resolution $\lambda/\Delta\lambda$
GRB 000210	0.8462	0.017	2009 November 20 084A-0631(A)	1.0 arcsec	1 × 2	UVB	1800 × 4	1.3	4000
					1 × 2	VIS	1800 × 4	1.5	5000
					1 × 1	NIR	600 × 12	1.5	2600
GRB 000418	1.1183	0.029	2010 April 16 085A-0795(A)	0.8 arcsec	1 × 2	UVB	1800 × 2	1.0	5400
					1 × 2	VIS	1800 × 2	0.9	8800
					1 × 1	NIR	600 × 6	0.9	5800
GRB 000911	1.0585	0.106	2009 November 21 084A-0631(A)	1.0 arcsec	1 × 2	UVB	1800 × 4	1.0	5300
					1 × 2	VIS	1800 × 4	0.9	8500
					1 × 1	NIR	600 × 12	0.9	5700
GRB 080413B	1.10124	0.032	2010 August 15 085A-0795(B)	0.6 arcsec	1 × 2	UVB	1800 × 3	1.0	4500
					1 × 2	VIS	1800 × 3	0.9	10000
					1 × 1	NIR	900 × 3	0.9	5700
GRB 100316B	1.181	0.124	2011 April 3 087A-0451(A)	1.3 arcsec	1 × 2	UVB	1200 × 4	0.8	6500
					1 × 2	VIS	1200 × 4	0.7	11000
					1 × 1	NIR	400 × 12	0.9	5700
GRB 100724A	1.289	0.038	2011 April 3 087A-0451(A)	0.8 arcsec	1 × 2	UVB	1200 × 4	0.8	6500
					1 × 2	VIS	1200 × 4	0.7	11000
					1 × 1	NIR	400 × 12	0.9	5700

Together, the GROND and IRAC data cover the rest-frame range of 220 nm to 1.7 μm and allow us to fit the SED using stellar population synthesis models. Here, we use models from Bruzual & Charlot (2003) and a Chabrier (2003) initial mass function (IMF) within Lephare (Arnouts et al. 1999; Ilbert et al. 2006). Our input models span a wide range of galaxy parameters as described in detail in Krühler et al. (2011). The host's photometric data are well described with a star-forming galaxy template with a B-band luminosity of $M_B = -19.4 \pm 0.3$ mag and a stellar mass of $\log(M_\star/\mathrm{M}_\odot) = 9.2^{+0.2}_{-0.4}$. Assuming the Baldry & Glazebrook (2003) IMF in the modelling, values of stellar mass are very similar to Chabrier (2003), therefore we use this value in further analysis.

2.2 Observations

We obtained X-Shooter spectra of the six LGRB hosts in the period between 2009 November and 2011 April. Slit positions with respect to the positions of the LGRB afterglows are shown in Fig. 1. All spectra were taken under dark sky, but different seeing conditions. In each case, the individual exposures were obtained by nodding along the slit with an offset of 5 arcsec between exposures in a standard ABBA sequence. Only two exposures (AB) were acquired in the case of GRB 000418 and only three (ABB) in the case of GRB 080413B due to clouds during both observations. Observation logs are given in Table 1.

2.3 Data reduction

We processed the spectra using version 2.0.0 of the X-Shooter data reduction pipeline (Goldoni et al. 2006; Modigliani et al. 2010), combined with the reduction technique developed for NODDING mode observations. The pipeline transforms the detected counts in physical quantities while propagating the errors and bad pixels consistently. First, the raw frames are subtracted from each other and cosmic rays are detected and removed using the method developed by van Dokkum (2001). The frames were divided by master flat-fields produced during day time with halogen lamps. Orders were extracted and rectified in wavelength space using the wavelength-spatial solution previously obtained from calibration frames. The resulting rectified frames were then shifted by the offset (5 arcsec), added and merged, thus the final 2D spectrum was obtained. The merging in the overlapping regions was weighted by the errors. The 1D spectrum together with the corresponding error file and bad pixel map, extracted at the source position from the 2D spectrum, are the final products of the pipeline. More than one source is found in the slit in the case of GRB 000911, therefore the reduction for this host was done separately for each nodding step using a STARE mode reduction. Individual extracted 1D products were averaged to obtain the final 1D spectrum.

The flux calibration of the spectra is particularly challenging for an instrument such as X-Shooter, which combines together three different detectors in UV, optical and NIR (e.g. see Krühler et al. 2015; Japelj et al. 2015). First, we used observations of a spectrophotometric standard star, taken on the same night as science spectra, to flux calibrate the spectra. The reduced standard star spectrum was divided by the tabulated spectrum to produce the response function: the response was interpolated in the atmospheric absorption regions in VIS and NIR spectra. The response function was then applied to the spectrum of the host. Flux values were subsequently cross-checked and corrected using the corresponding magnitudes of the galaxies. This was possible for GRB 000210, 000418 and 000911 hosts according to the photometric studies published in the literature.[2] Slit-aperture flux loss corrections are therefore included in the procedure.

[2] Published measurements were mainly taken from the public data base GHostS at www.grbhosts.org

Downloaded from http://mnras.oxfordjournals.org/ at CNR on December 9, 2015

Table 2. Emission-line fluxes (in units of 10^{-17} erg s^{-1} cm^{-2}) are corrected for Galactic extinction and stellar Balmer absorption (see Section 3 for details). Correction due to dust extinction in the host galaxies has not been applied. We report 3σ upper limits when lines are not detected. (a) If the [O II] doublet is clearly resolved, we report the flux for each line separately; (b) fluxes for the 'host' component (see Section 4.5 for details); (c) uncertain flux, but line is clearly detected in 2D; (d) see section 4 for details on the flux measurements; (e) undetected line falling on a sky line; (f) line falling in a telluric region; (g) there is a clear detection in 2D at the corresponding wavelength but the shape is different from the other lines; (h) line not detected in 2D. (i) line partially detected but strongly affected by a sky line.

Line	GRB 000210	GRB 000418	GRB 000911	GRB 080413B	GRB 100316B [(b)]	GRB 100724A
[O II]λ3726[(a)]	7.4 ± 0.4	3.6 ± 0.6	0.5 ± 0.1	0.8 ± 0.1	5.6 ± 0.4	1.0 ± 0.1
[O II]λ3729		5.1 ± 0.6	0.9 ± 0.1	1.0 ± 0.1		1.9 ± 0.1
[Ne III]λ3869	0.3 ± 0.2[(c)]	<1.1	<0.4	0.2 ± 0.1	<0.7	<0.7
Hγ	0.8 ± 0.3[(c)]	0.8 ± 0.3[(c)]	<0.4	0.2 ± 0.1[(g)]	0.6 ± 0.4[(h)]	<1.5
Hβ	2.2 ± 0.3	<7.2	<1.1	<2.2	<1.3	<1.3
[O III]λ4959	1.2 ± 0.3	5.4 ± 1.8	<3.4	[(e)]	2.6 ± 0.8	[(e)]
[O III]λ5007	4.7 ± 0.3	11.4 ± 1.8	<3.4	2.2 ± 0.3	[(i)]	2.8 ± 0.5
Hα	6.1[(d)]	[(f)]	[(f)]	1.4[(d)]	[(f)]	3.1 ± 0.4
[N II]λ6584	[(e)]	[(f)]	[(f)]	[(f)]	[(f)]	[(e)]

For the cases where the photometry is not available or the continuum is not detected, we checked the validity of flux calibration with telluric stars. Spectra of telluric stars were taken right after host observations and with the same instrumental setup (binning, slit width). Telluric stars were observed in the NODDING mode and the reduction procedure was the same as for the host spectrum. The same correction factors, obtained by comparing flux calibrated spectra of telluric stars to their magnitudes, were then applied to the spectra of the hosts. The method was tested in cases where magnitudes are available for both telluric stars and hosts: the uncertainty of this calibration (which does not include slit loss correction) is of the order of 20 per cent. This method was introduced and validated by Pita et al. (2014) who find similar conclusions. Due to the large uncertainty, we do not include slit-aperture flux loss corrections. The method was used to cross-calibrate the full spectra of GRB 080413B, 100316B and 100724A hosts.

3 MEASUREMENTS

The emission-line fluxes were measured using the code developed by us and cross-checked with the SPLOT task in IRAF.[3] In cases where a line is not detected, we report a 3σ upper limit. All fluxes are corrected for Galactic extinction in the direction of the host assuming the extinction curve of Cardelli, Clayton & Mathis (1989) and reddening values given in Table 1 (Schlafly & Finkbeiner 2011). Throughout the paper, we report line fluxes in units of 10^{-17} erg cm^{-2} s^{-1}.

Galaxies hosting young or intermediate age stellar populations feature strong Balmer absorption lines in their spectra. Thus, the Balmer emission lines are superimposed on the host stellar absorption lines (the absorption is typically negligible for metal lines). Due to a faint spectral continuum, we cannot detect the wings of absorption lines and therefore cannot correct for stellar absorption directly. Zahid, Kewley & Bresolin (2011) measured the average equivalent width (EW) of Hβ absorption line as a function of stellar mass and spectral resolution for a population of blue, low-mass galaxies, which is similar to the LGRB hosts of our sample. Given the X-Shooter resolution (Table 1) the results of Zahid et al. (2011) imply a typical rest-frame EW of stellar Hβ absorption line of 1 Å. We adopted this value to estimate the correction for the stellar absorption. The correction was non-negligible only for the Hβ line of GRB 100316B, where we estimate it to be $F_{\rm corr} = F_{\rm cont}(1+z)1\,\text{Å} \sim 0.2 \times 10^{-17}$ erg cm^{-2} s^{-1}.

Line fluxes, corrected for Galactic extinction and stellar absorption are reported in Table 2.

Dust extinction in the hosts is measured by comparing Balmer line ratios to theoretical expectations, calculated for nebular temperature of 10^4 K ($F_{\rm H\alpha}/F_{\rm H\beta} = 2.87$, $F_{\rm H\gamma}/F_{\rm H\beta} = 0.47$; Osterbrock & Ferland 2006). In the cases where Balmer lines are not detected, we searched through the literature for any estimate of dust extinction either from emission lines in the host-integrated signal or line of sight (via SED analysis of the afterglow). The details of host extinction correction for each host in our sample are given in Section 4 and the final adopted values are reported in Table 3. Dust-corrected emission-line fluxes are used in the analysis.

3.1 Star formation rates

Optical nebular lines effectively originate from the re-emission of stellar luminosity in galaxies at wavelengths shortwards of the Lyman limit, therefore directly probe the young, massive stellar populations (Kennicutt 1998). We estimated the SFR by using emission luminosities L from dust-extinction and stellar-absorption-corrected Hα, Hβ and [O II] line fluxes and the following prescriptions:

$$\mathrm{SFR_{H\alpha}} = 4.39 \times 10^{-42} \frac{L_{\rm H\alpha}}{\text{erg s}^{-1}} \mathrm{M_\odot\ yr^{-1}}, \quad (1)$$

$$\mathrm{SFR_{H\beta}} = 12.6 \times 10^{-42} \frac{L_{\rm H\beta}}{\text{erg s}^{-1}} \mathrm{M_\odot\ yr^{-1}}, \quad (2)$$

$$\mathrm{SFR_{[O\,II]}} = 5.54 \times 10^{-42} \frac{L_{\rm [O\,II]}}{\text{erg s}^{-1}} \mathrm{M_\odot\ yr^{-1}}, \quad (3)$$

where the relation for Hα line is the one reported by Kennicutt (1998), but divided by a factor of 1.8 to go from Salpeter IMF (Salpeter 1955) to a more realistic IMF (Baldry & Glazebrook 2003). SFR for Hβ is obtained by using the Balmer decrement at typical nebular temperatures of 10^4 K (Hα/Hβ = 2.87). The [O II] SFR relation is the one empirically derived specifically for LGRB hosts by Savaglio et al. (2009). The advantage of using the [O II] as a tracer of SFR is that this line is usually stronger than Hβ and easy to detect. However, it is more affected by dust extinction.

[3] IRAF is software distributed by *National Optical Astronomy Observatories*.

Downloaded from http://mnras.oxfordjournals.org/ at CNR on December 9, 2015

Table 3. Host parameters measured from detected lines (Table 2): host extinction, metallicities from different calibrations, SFR and electron density. Measurement details for each specific galaxy are given in Section 4. In the last column, we add values of hosts' stellar masses, when available. (a) M91, KK04 and P05 metallicities are based on the degenerate R_{23} calibration, thus both solutions are reported. Metallicity errors do not include calibration uncertainties (see text); (b) the theoretical Balmer decrement $F_{H\beta} = F_{H\alpha}/2.87$ is assumed.

		$12 + \log(O/H)^{(a)}$				SFR ($M_\odot$ yr^{-1})					
Host	A_V	M91	KK04	P05	[Ne III]/[O II]	M08	Hα	Hβ	[O II]	n_e (cm^{-3})	log ($M_*/M_\odot$)
000210	0	8.1 ± 0.1 8.6 ± 0.1	8.2 ± 0.1 8.7 ± 0.1	7.9 ± 0.2 8.2 ± 0.1	8.7 ± 0.2	8.6 ± 0.1	~ 0.9	1.0±0.1	1.4±0.1		$9.31^{+0.08}_{-0.08}$
000418	1.3	~8.4	~8.4		>8.3	>8.3		<25.4	19.0±1.9	<100	$9.26^{+0.14}_{-0.14}$
000911	0.4				>7.9	8.1±0.6		<1.3	0.8±0.2	<10	$9.32^{+0.26}_{-0.26}$
080413B$^{(b)}$	0	~8.4	~8.4	~8.4	8.4 ± 0.2	8.4 ± 0.2	0.4 ± 0.1	<1.9	0.7±0.1	<30	$9.2^{+0.2}_{-0.4}$
100316B	0	~8.4	~8.4		>8.3	>7.9		<1.3	2.5±0.2		
100724A	0	8.0 ± 0.1 8.6 ± 0.1	8.2 ± 0.1 8.8 ± 0.1	7.9 ± 0.2 8.3 ± 0.1	>8.0		1.4 ± 0.2	<1.6	1.6 ± 0.1		

Moreover, [O II] depends on the metallicity and ionization level. Nevertheless, Savaglio et al. (2009) showed that it can still be quite reliable and thus a valuable tool in case the two hydrogen lines are contaminated or undetected.

We measure SFRs for all six hosts in the sample. SFR values are reported in Table 3.

3.2 Metallicities

Emission lines in HII regions have been used for a long time to derive metallicities in the ionized interstellar medium (ISM) of galaxies. A number of metallicity calibrations have been developed in the past three decades (see Kewley & Ellison 2008 for a review). The calibrations were derived either with the help of theoretical models or from empirical relations or from a combination of the two. In all cases, the metallicity can be estimated by using relations that are a function of different combinations of emission-line flux ratios. Unfortunately, each method is affected by systematic errors, which may also be function of redshift (ionization is perhaps the evolving physical parameter). When comparing the metallicity of different objects it is therefore important to measure the metallicities with the same calibration method.

According to the line set available, we can use two calibrations which are based on theoretical photoionization models (M91 – McGaugh 1991; KK04 – Kobulnicky & Kewley 2004) and on two empirical calibrations (P05 – Pilyugin & Thuan 2005; [Ne III]/[O II] – Maiolino et al. 2008). M91, KK04 and P05 calibrations rely on the so-called R_{23} parameter, defined as:

$$R_{23} = \frac{[\mathrm{O\,II}]\lambda3727 + [\mathrm{O\,III}]\lambda4959 + [\mathrm{O\,III}]\lambda5007}{\mathrm{H}\,\beta}, \quad (4)$$

where the [O II]λ3727 is the total flux of the doublet. All these lines are usually strong and easily detectable. The calibrations could have problems if the host extinction is not properly taken into account. The R_{23} has one major drawback: it gives two solutions for the metallicity, the upper- and the lower-branch solution. The most probable metallicity can be chosen by cross-correlating with additional information, for instance if the [N II]/[O II] or [N II]/Hα ratio – both strong functions of metallicity (Kewley & Dopita 2002; Kewley & Ellison 2008) – is measured. In our sample, these two ratios are not available. In the KK04 calibration, an additional parameter considered in the R_{23} relation is the ionization defined by the line ratio $O_{32} = [\mathrm{O\,III}]\lambda4959, 5007/[\mathrm{O\,II}]\lambda3727$. In the KK04 calibration, the ionization parameter in the lower- and upper-branch solution is obtained iteratively. The O_{32} ratio itself can be used to choose the branch of R_{23} (Nagao, Maiolino & Marconi 2006; Maiolino et al. 2008). The P05 calibration includes the excitation parameter $P = ([\mathrm{O\,III}]\lambda4959, 5007/\mathrm{H}\,\beta)/R_{23}$. Another useful calibration uses the line ratio [Ne III]λ3869/[O II]λ3727 (Maiolino et al. 2008). This ratio has the advantage that the lines are very close, and the dust correction has a minimal effect, therefore it is a valuable method when extinction is unknown. Moreover, in contrast to the other three methods used in this work, its solution is unique (but it is sensitive to the ionization parameter). Uncertainties for M91, KK04, P05 and [Ne III]/[O II] calibrations are estimated to be 0.15, 0.15, 0.1 and 0.15 dex, respectively. All measured metallicities are summarized in Table 3.

We also measure metallicities by simultaneously considering all flux ratios between relevant emission lines and fitting them with two free parameters: metallicity and host extinction (M08; Maiolino et al. 2008). In the case of a good data set, this method can surpass problems faced by individual line ratios (e.g. double valued solution of R_{23} calibrator or poorly known extinction). Most of the relevant lines have been measured for the GRB 000210 and 080413B hosts, for which we measure a negligible host extinction and metallicities of 12+log(O/H) of 8.6 ± 0.1 and 8.4 ± 0.2, respectively. All the other hosts lack detection of the Hβ line, and in the two cases where the Hα is detected, [N II]λ6584 is not. This makes the measurement of metallicity problematic. Limits or rough estimates can be obtained from O_{32} for GRB000418 and GRB100724A and from upper and lower limits to flux ratios for the others.

3.3 Electron densities

The doublet [O II]λ3726, 3729 line ratio is sensitive to the electron density in the gas n_e (Osterbrock & Ferland 2006). For those hosts with resolved [O II] lines, the electron density is estimated by assuming a typical temperature in the star-forming region $T \sim 10^4$ K (fig. 5.8 in Osterbrock & Ferland 2006). We were only able to measure upper limits on n_e: the results are shown in Table 3.

4 RESULTS

In the following, we present detailed results for each individual host discussing both the characteristics already published and the new X-Shooter results. As an example of X-Shooter spectra, we show the figures of 1D and 2D spectra in the proximity of detected lines for GRB 000210 host. SFRs and stellar masses are reported assuming a Baldry & Glazebrook (2003) IMF.

Downloaded from http://mnras.oxfordjournals.org/ at CNR on December 9, 2015

4.1 GRB 000210 host

The X-Shooter spectrum of the GRB 000210 host galaxy reveals several emission lines: [O II], [Ne III], Hγ, Hβ, [O III] and Hα (Figs 2 and 3). The Hα line is marginally contaminated by a sky line. Considering the shape and the velocity spread (about 250 km s^{-1}) of the lines, we could estimate the amount of missing flux and apply the correction. The derived values are consistent with theoretical Hα/Hβ and Hα/Hγ ratios, expected for a negligible (within errors) dust extinction. Negligible dust extinction is also derived by the modelling of the host SED with synthetic galaxy spectra (Gorosabel et al. 2003a). GRB 000210 was classified as dark and even though a typical dark GRB host is significantly dust obscured, there are known cases of dark GRB hosts with very low or even negligible host-averaged dust extinction (Perley et al. 2013; Krühler et al. 2011).

Hα, Hβ and [O II] line fluxes give SFR = $\sim$0.9, 1.0 $\pm$ 0.1 and 1.4 $\pm$ 0.1 M$_\odot$ yr^{-1}, respectively. These values are a factor $\sim$2 lower than the ones reported by Savaglio et al. (2009). The discrepancy is due to the average dust-extinction correction (with $A_V = 0.53$) applied by Savaglio et al. (2009) for all hosts in their sample which had no dust-extinction estimate. On the other hand, the UV continuum-based SFR obtained by Savaglio et al. (2009) SFR$_{2800} \approx 1.34$ M$_\odot$ yr^{-1}, is similar to our results.

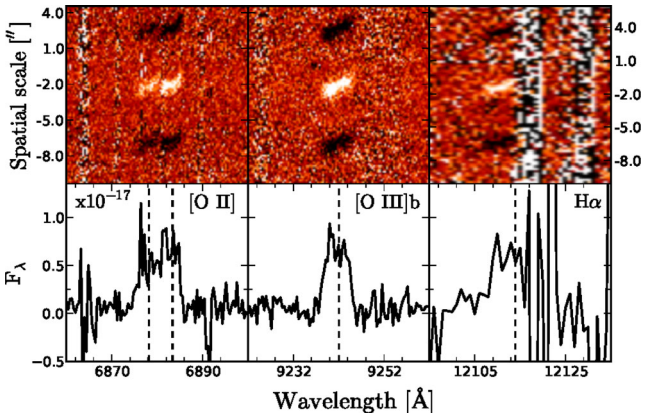

Figure 2. [O II], [O III]λ5007 and Hα lines as observed by the X-Shooter for GRB 000210 host. Both 2D (up) as well as extracted 1D (bottom) spectra are plotted for each line. In general, spatial and wavelength scale of VIS and NIR differ. Vertical dashed lines show redshifted air wavelengths of corresponding lines. Flux calibration of 1D spectra is not scaled with respect to photometric measurements or telluric stars (see Section 2).

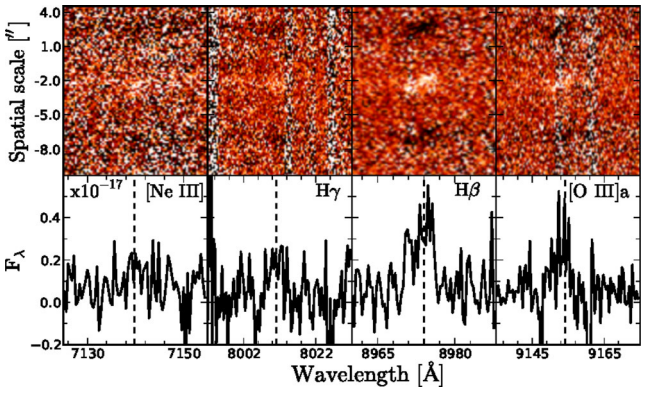

Figure 3. [Ne III], Hγ, Hβ and [O III]λ4959 lines as observed by the X-Shooter for GRB 000210 host.

R_{23}-based metallicities are measured to be 8.1 $\pm$ 0.1, 8.2 $\pm$ 0.1, 7.9 $\pm$ 0.2 for lower-branch, and 8.6 $\pm$ 0.1, 8.7 $\pm$ 0.1, 8.2 $\pm$ 0.1 for upper-branch solution by using the M91, KK04, P05 calibrators, respectively. Since [N II] is not detected, we cannot break the degeneracy. Nagao et al. (2006) and Maiolino et al. (2008) showed that, in the absence of [N II], the [O III]λ5007/[O II]λ3727 ratio could be used instead. We measure [O III]λ5007/[O II]λ3727 $\sim$ 0.7, which together with the [Ne III]λ3869/[O II]λ3727 ratio are only consistent with the upper-branch solution. Additionally, the rich line data set allows us to use the M08 method to measure metallicity and extinction of the host: the best-fitting parameters of the multiple line ratios fit are $Z_{M08} = 8.6 \pm 0.1$ and $A_V \sim 0$.

[O II] doublet is barely resolved (Fig. 2), therefore we do not attempt to measure the average electron density in H II regions.

Using the SFR from Hα and a stellar mass of $M_* \sim 10^{9.31}$ M$_\odot$ from Savaglio et al. (2009), we calculate an sSFR, SFR/M_* = sSFR $\approx$ 0.4 Gyr^{-1}, which is consistent with the one derived for other LGRB hosts at $z \sim 1$ (Hunt et al. 2014).

4.2 GRB 000418 host

We detect four emission lines with X-Shooter: [O II], Hγ and the [O III] doublet spanning a velocity range of about 190 km s^{-1}. We do not detect Hα and only poorly constrain the upper limit for Hβ (which falls on the edge of the NIR arm), therefore we cannot use Balmer line ratios to determine host extinction. To correct our flux values for host extinction, we adopt the value of $A_V = 1.3$, which is the average host optical extinction found by Perley et al. (2013) and Schady et al. (2014) (similar extinction of 0.96 $\pm$ 0.20 has been measured in the GRB line of sight by Klose et al. 2000).

[O II] gives SFR =19.0 $\pm$ 1.9 M$_\odot$ yr^{-1} (consistent with the Hβ upper limit). The lower limit to [O II]/Hβ and upper limit to [Ne III]/[O II] together with a measure of [O III]/[O II], gives a metallicity 12 + log (O/H) $>$ 8.2 with the M08 method. For R_{23} metallicities, we use Hγ to estimate $F_{H\beta} = F_{H\gamma}/0.47 = (2.7 \pm 1.0) \times 10^{-17}$ erg s^{-1} cm^{-2}. In the case of M91 and KK04 calibrators, the R_{23} value is at the turnover point (log $R_{23} = 1$; Kobulnicky & Kewley 2004) meaning that the metallicity is 12 + log (O/H) $\sim$ 8.4, equivalently for M91 and KK04 calibrators. In the case of P05, the solution is unphysical (log $R_{23} > 1$). We note that Hγ is only tentatively detected (2.7σ significant) and the measured flux highly uncertain.

Taking errors into account, we conservatively measure the electron density for this host as $n_e < 100$ cm^{-3}. Using our measured value of SFR$_{[O II]}$ and a stellar mass $M_* \sim 10^{9.26}$ M$_\odot$ (Savaglio et al. 2009), we calculate sSFR $\approx$ 3.1 Gyr^{-1}.

4.3 GRB 000911 host

We could identify in the spectra three emission-line sets: one of the host galaxy at $z = 1.058$, one at $z = 0.646$ at a position about 4.5 arcsec NE of the host ([O II], Hβ, [O III], Hα) and a third one at $z = 0.823$, about 1.8 arcsec SW from the host, for which only the [O III] doublet is detected. The galaxy at $z = 0.646$ would contaminate the host spectrum in a NODDING mode reduction, therefore we reduced the host spectrum in a STARE mode.

Only the [O II] doublet is detected for the LGRB host, spanning about 130 km s^{-1}. Hα falls in a telluric absorption band, and Hβ and [O III] are in a very noisy part at the beginning of the NIR spectrum, therefore we can determine only flux limits. To correct the [O II] fluxes for host extinction, we use $A_V = 0.4$ and a Large Magellanic Cloud extinction curve (Masetti et al. 2005) – the value is consistent

Downloaded from http://mnras.oxfordjournals.org/ at CNR on December 9, 2015

within errors with the GRB line-of-sight host extinction measured to be $A_V = 0.27 \pm 0.32$ (Kann, Klose & Zeh 2006).

We measured $SFR_{[O\,II]} = 0.8 \pm 0.2\,M_\odot\,yr^{-1}$, which is lower than previous measurements based on the [O II] line, but in agreement with the UV continuum-based SFR_{2800} found by Savaglio et al. (2009). Due to the sparsity of detected lines and the limits found on [O III]/[O II], [O II]/Hβ and [Ne III]/[O II] we were only able to determine a lower limit to the metallicity $12 + \log(O/H) > 7.9$ based on the [Ne III]/[O II] calibration method, while the M08 method resulted in an unconstrained valued.

The electron density is measured to be $n_e < 10\,cm^{-3}$. Using our measured SFR and a stellar mass $M_* \sim 10^{9.32}\,M_\odot$ (Savaglio et al. 2009), we calculate $sSFR_{[O\,II]} \approx 0.4\,Gyr^{-1}$.

4.4 GRB 080413B host

Five emission lines are detected in the X-Shooter spectrum of the GRB 080413B host: [O II] doublet, [Ne III], Hγ, [O III]λ5007 and Hα spanning about 130 km s^{-1}. Lines are found to originate at a common redshift $z = 1.10124$, consistent with the redshift $z = 1.1014$ found from the afterglow spectrum (Fynbo et al. 2009), therefore confirming association of detected emission lines with the GRB 080413B host galaxy.

The Hα line is detected, but strongly affected by the telluric absorption. We used the spectrum of the telluric star observed right after the host to extract the telluric spectrum and correct the region around Hα (the corrected flux is reported in Table 2). We caution that the spectrum of the telluric star was taken at different airmass than the spectrum of the host, adding some extra uncertainty to the reported flux. We note that the measured value $F_{H\alpha} \approx 1.4 \times 10^{-17}$ erg s^{-1} cm^{-2} is very close to the one expected from the detected Hγ (i.e. $F_{H\alpha} \approx 6 \times F_{H\gamma} \approx 1.2 \times 10^{-17}$ erg s^{-1} cm^{-2}).

The dust extinction could not be determined from the Balmer decrement. Filgas et al. (2011) studied the afterglow of GRB 080413B and found that the sightline host extinction is negligible. Thus, we do not apply any dust-extinction correction.

[O II] and Hα lines are used to measure $SFR = 0.7 \pm 0.1\,M_\odot\,yr^{-1}$ and $SFR = 0.4 \pm 0.1\,M_\odot\,yr^{-1}$, respectively. The detection of [Ne III], [O II] and [O III] enables us to measure the M08 metallicity $12 + \log(O/H) = 8.4 \pm 0.2$. Since the weakest line of the [OIII] is not detected, we assume the theoretical line ratio and estimate $F_{[O\,III]\lambda4959} = F_{[O\,III]\lambda5007}/3 = 0.7 \pm 0.3$ (Storey & Zeippen 2000). We infer Hβ flux from Hα: $F_{H\beta} = F_{H\alpha}/2.87 \approx 0.5 \times 10^{-17}$ erg s^{-1} cm^{-2}. According to all three R_{23} calibrators the solution is consistent, within errors, with the turnover point at $\log R_{23} = 1$ (Kobulnicky & Kewley 2004), that is, $12 + \log(O/H) \sim 8.4$ which is very close to the measured M08 metallicity.

The electron density is estimated to be $n_e < 30\,cm^{-3}$. Using our measured SFR and stellar mass we calculate $sSFR_{[O\,II]} \approx 0.4\,Gyr^{-1}$.

4.5 GRB 100316B host

In the X-Shooter spectra of the host, a strong [O II] doublet spreading more than 450 km s^{-1} is clearly detected at the afterglow coordinates. Its profile is asymmetric. There is also a continuum trace clearly detected all along the spectra, centred about 1 arcsec below the afterglow coordinates. Due to the lack of deep images of the field and poor seeing conditions during observations, it is not possible to determine if the line emission and continuum belong to the same system. None the less, the spatial profile of the [O II] doublet in the 2D spectrum seems to indicate a second smaller peak at the continuum centre, suggesting the presence of one single galaxy with a particularly active region, or two close galaxies at the same redshift one of which faint and star forming (that at the afterglow position) and the other brighter and less active. Deep observations of the host and ideally high spatially resolved Integral Field Unit (IFU) spectroscopy could give information on this interesting system.

For our analysis we extracted two sets of 1D spectra: one centred on the [O II] doublet detected at the afterglow position (called here HOST and whose fluxes are reported in Table 2) and with a spatial coverage as large as the seeing (1.3 arcsec), and the other including also the continuum region (hereafter 'TOT'). For the HOST system, we detect also [O III]. The noise in the TOT spectra is much higher and we can report only limits for this line. No other lines are detected. The [O II] doublet flux in the TOT extraction is 8.1 ± 0.5^{-17} erg s^{-1} cm^{-2}.

[O II] doublet, Hγ and [O III] lie at a common redshift of $z = 1.181$, consistent with the redshift $z = 1.180$ found for the afterglow spectroscopy (Vergani et al. 2010).

Greiner et al. (2011) studied the afterglow of GRB 100316B and found that the sightline host extinction is negligible. A negligible extinction is also inferred from the detected Hγ and Hβ upper limit. We thus assume $A_V \sim 0$ for the host extinction.

From the [O II] emission line we measure a HOST $SFR_{[O\,II]} = 2.5 \pm 0.2\,M_\odot\,yr^{-1}$. We were able to determine a lower limit to the metallicity $12 + \log(O/H) > 8.3$, 7.9 based on the [Ne III]/[O II], M08 calibration, respectively. Even though Hγ is only tentatively detected, we can use it to estimate the metallicity from R_{23} by assuming $F_{H\beta} = F_{H\gamma}/0.47 \sim 1.3$. We also assume $F_{[O\,III]\lambda5007} = 3 \times F_{[O\,III]\lambda4959} = 7.8 \pm 2.3$. In the case of M91 and KK04 calibrators, the solution is consistent, within errors, with the turnover point at $\log R_{23} = 1$ (Kobulnicky & Kewley 2004), that is, $12 + \log(O/H) \sim 8.4$. For the P05 calibration, the solution is unphysical ($\log R_{23} > 1$).

The [O II] doublet is not resolved, therefore we cannot measure the average electron density in H II regions.

4.6 GRB 100724A host

Three emission lines are detected in the X-Shooter spectrum: the [O II] doublet, [O III]λ5007 and Hα, spanning about 200 km s^{-1}. Lines are found to originate at a common redshift $z = 1.289$, consistent with the redshift $z = 1.288$ found from the afterglow spectroscopy (Thöne et al. 2010). Even though the continuum is not detected in the NIR arm, upper limits on the continuum are so low that the correction to the measured flux values is completely within the estimated errors. Hβ and Hγ are too loosely constrained to provide any constraint on the host extinction. Since there are no other observations and data on the host dust extinction in the literature, we neglect the dust extinction.

Hα and [O II] lines are used to estimate $SFR = 1.4 \pm 0.2$ and $SFR = 1.6 \pm 0.1\,M_\odot\,yr^{-1}$, respectively. Because we do not know the extinction in the host, these values are formally lower limits. We were able to determine a lower limit to the metallicity $12 + \log(O/H) > 8.0$ based on the [Ne III]/[O ii] calibration. For R_{23}, we assume $F_{[O\,III]\lambda4959} = F_{[O\,III]\lambda5007}/3 = 0.9 \pm 0.2$ and $F_{H\beta} = F_{H\alpha}/2.87 = 1.1 \pm 0.1$. Thus, the R_{23}-based metallicities are 8.0 ± 0.1, 8.2 ± 0.1 and 7.9 ± 0.2 for the lower-branch solution, and 8.6 ± 0.1, 8.8 ± 0.1 and 8.3 ± 0.1 for the upper-branch solution, for M91, KK04 and P05, respectively. We note that the value of Hβ obtained in this case is much more reliable than the

Downloaded from http://mnras.oxfordjournals.org/ at CNR on December 9, 2015

one inferred from Hγ for other hosts, because Hα is detected with high significance.

Even though the [O II] doublet is resolved, we cannot put constraints on the electron density measurement other than to say it is most likely very low, because the line ratio ($F_{[\mathrm{O\,II}]\lambda3729}/F_{[\mathrm{O\,II}]\lambda3726} = 1.9 \pm 0.2$) is outside the range predicted by theoretical calculation (see Section 3.3 for our assumptions and references).

5 DISCUSSION

From the analysis performed on these six LGRB host galaxies with $0.846 < z < 1.289$, it is clear how the VLT/X-Shooter spectrograph can observe emission lines which are generally difficult to detect because either the emission lines of the object fall in the gap between optical and NIR ranges and/or for the inadequate sensitivity of earlier spectrographs. X-Shooter allows the detection of a more complete set of emission lines and this is a fundamental prerogative for the determination of the main features of galaxies even at high redshift.

In particular, with the galaxies analysed in this work, it was possible to determine the values of metallicity and SFR using different indicators, allowing us to add information about the reliability of these methods also at redshift greater than 1. In addition, with the spectra, which were particularly rich in emission lines, it was possible to obtain the extinction value using both the Balmer lines and the gas electron density from the components ratio of the [O II] doublet. Finally, by using the stellar-mass values provided by literature or by us, we also studied the mass–metallicity (M–Z) relation and the sSFR for some of these LGRB host galaxies.

The hosts included in our sample are quite diverse in their properties (e.g. two galaxies hosted a dark GRB), however, given our selection methods (see Section 2.1), the sample is small and inhomogeneous, preventing us to draw strong conclusions regarding the population of GRB hosts as a whole. For the latter studies of complete samples are imperative (e.g. Hjorth & Bloom 2012; Vergani et al. 2014; Krühler et al. 2015; Perley et al. 2015a). We therefore discuss our results within the framework of already known properties of LGRB hosts.

5.1 SFR and metallicity of two dark-LGRB hosts

The high extinction of the afterglow of GRB 000210 and the non-detection of the optical afterglow of GRB 000418 put these two LGRBs in the class of dark bursts (but see Schady et al. 2014). In the last years, many works tackled the properties of dark burst host galaxies to test whether they were similar to those of non-dark LGRBs, since the presence of a substantial amount of dust could indicate more evolved hosts than those previously usually found in LGRB host galaxy studies. Dark-LGRB host galaxies tend to have on average larger stellar masses and luminosities than non-dark-LGRB host galaxy population (Hunt et al. 2014; Krühler et al. 2011; Perley et al. 2013). Another topic of interest in those studies is to retrieve information on the dust distribution in high-redshift star-forming galaxies. The dust that caused the extinction of the burst could just be concentrated in small clouds around the exploding star or along the LGRB line of sight or be largely present in the entire galaxy. Covino et al. (2013) showed that lines of sight towards dark bursts have higher extinctions than the average extinction measured for non-dark population. The extinction inferred from the Balmer line ratio and/or the optical/NIR SED of the host galaxies of GRB 000210 and GRB 000418 (we measured A_V for this) is low. Their SFR and metallicity determined from the optical emission lines are not high (though see the different values found for GRB 000210) and typical of LGRB hosts. On the other hand, sub-mm and radio studies (Michałowski et al. 2008) showed that they have a large amount of obscured SFR. All this can be explained if the optical and sub-millimetre emission of the hosts are dominated by different populations of stars, as can be in young hosts experiencing a starburst episode (see Michałowski et al. 2008; Perley et al. 2013, 2015b). If sub-solar[4] metallicities are typically found in general also for the dark-LGRB host galaxies, we could have a further evidence that LGRBs prefer low-metallicity environments. Detailed studies on a larger population of dark burst host galaxies are needed.

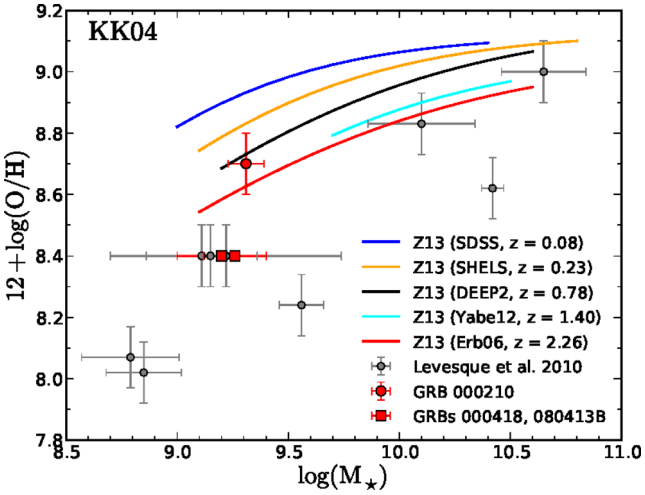

Figure 4. Stellar mass–metallicity relation for different galaxy samples. Coloured curves are fits to five samples of galaxies lying at different redshifts in the range of ∼0.1–2.3 (Zahid et al. 2013). Grey circles represent long GRB host galaxies in the redshift interval $0.3 < z < 1$ (Levesque et al. 2010). Included are host galaxies of GRB 000210 (filled point corresponds to the upper-branch solution), GRB 000418 and GRB 080413B, for which we have measurements of both mass and metallicity. All metallicities in this plot correspond to the Kobulnicky & Kewley (2004) R_{23} diagnostic.

5.2 Mass–metallicity relation

In Fig. 4, we show the M–Z relation of a number of GRB hosts, including the metallicities of our three LGRB host galaxies for which we measured metallicity and have stellar masses from the literature (GRB 000210, GRB 000418) and from our measurements (GRB 080413B). These values were compared with the results obtained from the analysis that Levesque et al. (2010) carried out on a sample of LGRB of redshift $z < 1$ together with five samples of galaxies lying at different redshifts in the range of ∼0.1–2.3 (Zahid et al. 2013). All metallicities in this plot correspond to the Kobulnicky & Kewley (2004) R_{23} diagnostic.

As justified in Section 4.1, in the case of GRB 000210 we can use the upper-branch solution for metallicity determined with the R_{23} calibration methods. For this host all calibrations return us the near-solar metallicity of $12 + \log(\mathrm{O/H}) \sim 8.6$, which is in agreement with the general M–Z relation for star-forming galaxies (see Fig. 4). GRB hosts with solar or supersolar metallicity are

[4] For solar metallicity, we assume the value of $12 + \log(\mathrm{O/H}) = 8.69$ (Asplund et al. 2009).

Downloaded from http://mnras.oxfordjournals.org/ at CNR on December 9, 2015

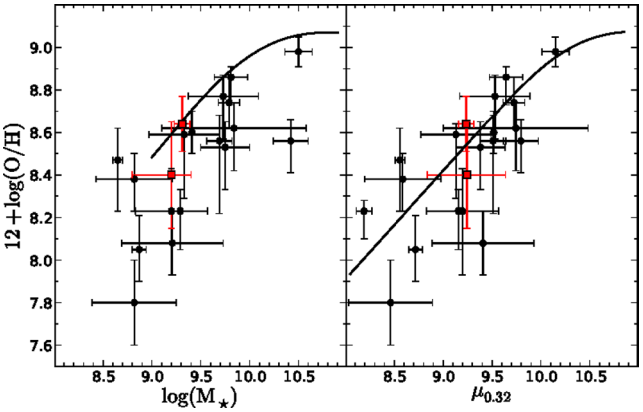

Figure 5. Left: gas metallicity as a function of stellar mass $M_\star$. The black points represent the sample of long GRB host galaxies used by Mannucci et al. (2011). The position of GRB 000210 and GRB 080413B hosts in the plot is given by the red squares. The black line is a fit to the mass–metallicity relation for local galaxies (Mannucci et al. 2010). Right: gas metallicity as a function of $\mu_{0.32} = \log(M_\star) - 0.32\log(\mathrm{SFR})$. The black line is the extended fundamental metallicity relation, presented in Mannucci et al. (2011).

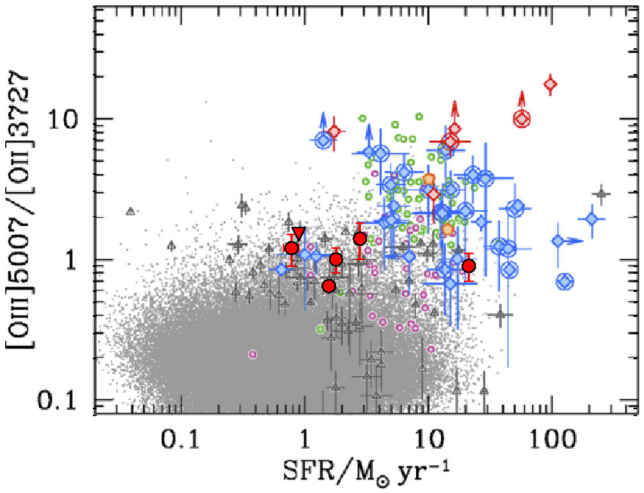

Figure 6. Dependence of [O III]λ5007/[O II] on SFR for our six hosts (red points, triangle marks an upper limit for the host of GRB 000911). Also plotted are data from Nakajima & Ouchi (2014): SDSS galaxies (grey points); red and blue diamonds represent $z = 2$–3 Lyman α emitters and Lyman-break galaxies, respectively (diamonds with circles denote $z > 3$ galaxies); grey triangles are $z \sim 1$ star-forming galaxies; green and purple circles show Green Pea galaxies and Lyman break analogues, while the orange pentagons are Lyman continuum leakers in the Local Universe. To convert our SFR values to Chabrier (2003) IMF, we multiplied them by a factor of 1.2.

not unprecedented (Savaglio 2010; Levesque et al. 2010). In fact, Krühler et al. (2015), analysing a large (inhomogeneous) sample of 96 GRB hosts found that ∼20 per cent of GRB hosts have supersolar metallicities. While this demonstrates that not all the environments in which LGRBs explode must necessarily be characterized by low metallicity, a general GRB host population (at least at $z < 1.5$) is still inclined to be metal poor (Graham & Fruchter 2013; Vergani et al. 2014; Krühler et al. 2015; Perley et al. 2015c). Hosts of GRBs 000418 and GRB 080413B are found to have metallicities that lie below the general star-forming galaxy population.

5.3 Fundamental metallicity relation

Mannucci et al. (2010) showed that a general relation between stellar mass, metallicity and SFR (i.e. fundamental metallicity relation or FMR) exists at least up to $z \sim 2.5$. The evolution of *M–Z* relation with redshift, as shown in Fig. 4 can therefore be attributed to the fact that galaxies at progressively higher redshifts have higher SFR and consequently lower metallicities. Furthermore, Mannucci et al. (2011) showed that the FMR relation also holds for LGRB host galaxies, implying that the stellar mass, metallicity and SFR within these galaxies are related in the same way as in the population of field galaxies. This is not at odds with the findings that LGRBs are preferentially found in galaxies of low metallicities. In Fig. 5, we show the FMR for a sample of host galaxies, including the GRB 000210 and GRB 080413B hosts. The two hosts from our sample are in good agreement with the FMR by Mannucci et al. (2011).

5.4 Star formation rate

In Fig. 6, we present the dependence of [O III]λ5007/[O II] on SFR for our six hosts (red points, triangle marks an upper limit for the host of GRB 000911) together with the data from Nakajima & Ouchi (2014) for several other types of galaxies. The [O III]λ5007/[O II] ratio is a proxy for ionization parameter and metallicity: higher oxygen ratio corresponds to lower metallicity and higher ionization parameter (e.g. see fig. 2 in Nakajima & Ouchi 2014). Our six LGRB hosts occupy the same part of the region as a population of star-forming galaxies at $z \sim 1$. However, while other star-forming galaxies are found in a wide parameter space, LGRB hosts are found in a rather narrow region that, according to the photoionization models of Kewley & Dopita (2002), are consistent with low metallicities and low ionization parameters.

6 SUMMARY AND CONCLUSIONS

We present VLT/X-Shooter data and results of six GRB host galaxies in the redshift range of $0.8 < z < 1.3$. Thanks to X-Shooter capabilities and resolution, we were able to measure the common bright emission lines in the majority of our hosts in order to better characterize the six GRB host galaxies at $z < 1$. From the emission-line measurements, we were able to derive properties like dust extinction, SFR, metallicities and electron densities where possible. In particular, we measured SFR and metallicities for all the hosts of the sample. Only three host masses where available, therefore, regarding the *M–Z* relation based on the three hosts measurements, we found that one host fall in the general *M–Z* relation of star-forming galaxies and two of them are found to lie below this relation. These hosts have metallicities around solar or below solar, which is consistent with the growing evidence for a metallicity threshold around this value. The two dark GRB hosts are found to have low host-averaged extinctions and SFRs, derived from optical emission lines, that are much lower than the ones measured from the sub-mm and radio studies (Michałowski et al. 2008). This may be an indication of different stellar populations and ISM properties which contributed to the emission at different wavelengths and shows the necessity for multiwavelength studies if we are to understand the hosts' properties in detail. Moreover, the two hosts for which we have stellar mass, metallicity and SFR are found to be in good agreement with the FMR relation by Mannucci et al. (2011). Comparing SFR measurements from our six hosts with several samples of galaxies we found that they occupy the same region as a star-forming galaxy population at $z \sim 1$.

Downloaded from http://mnras.oxfordjournals.org/ at CNR on December 9, 2015

ACKNOWLEDGEMENTS

This work is based on VLT/X-Shooter spectroscopy observations performed at the European Southern Observatory, Paranal, Chile. We acknowledge ESO personnel for their assistance during the observing runs and Roberto Pallavicini, the Italian P.I. of X-Shooter, who was one of the most active promoters of this wonderful instrument. We thank Tommaso Vinci with his software Identifica. SP acknowledges partial support from PRIN MIUR 2009 and from ASI INAF I/004/11/1. E. Pian acknowledges financial support from MIUR and Scuola Normale Superiore, and from grants ASI INAF I/088/06/0 and INAF PRIN 2011. This research has made use of the GHostS data base (www.grbhosts.org), which is partly funded by *Spitzer*/NASA grant RSA Agreement No. 1287913. This paper is based on observations collected at the European Southern Observatory Very Large Telescope, Cerro Paranal, Chile (programmes 084.A-0631(A), 085A-0795(A) and 0.87A-0451(A)).

REFERENCES

Arnouts S., Cristiani S., Moscardini L., Matarrese S., Lucchin F., Fontana A., Giallongo E., 1999, MNRAS, 310, 540
Asplund M., Grevesse N., Sauval A. J., Scott P., 2009, ARA&A, 47, 481
Baldry I. K., Glazebrook K., 2003, ApJ, 593, 258
Barnard V. E. et al., 2003, MNRAS, 338, 1
Berger E., Cowie L. L., Kulkarni S. R., Frail D. A., Aussel H., Barger A. J., 2003, ApJ, 588, 99
Boissier S., Salvaterra R., Le Floc'h E., Basa S., Buat V., Prantzos N., Vergani S. D., Savaglio S., 2013, A&A, 557, A34
Bruzual G., Charlot S., 2003, MNRAS, 344, 1000
Calzetti D., Armus L., Bohlin R. C., Kinney A. L., Koornneef J., Storchi-Bergmann T., 2000, ApJ, 533, 682
Campisi M. A., Tapparello C., Salvaterra R., Mannucci F., Colpi M., 2011, MNRAS, 417, 1013
Cardelli J. A., Clayton G. C., Mathis J. S., 1989, ApJ, 345, 245
Chabrier G., 2003, PASP, 115, 763
Covino S. et al., 2013, MNRAS, 432, 1231
Della Valle M. et al., 2006, Nature, 444, 1050
Elliott J. et al., 2013, A&A, 556, A23
Filgas R. et al., 2011, A&A, 526, A113
Fitzpatrick E. L., 1986, AJ, 92, 1068
Fynbo J. P. U. et al., 2006, Nature, 444, 1047
Fynbo J. P. U. et al., 2009, ApJS, 185, 526
Gal-Yam A. et al., 2006, Nature, 444, 1053
Galama T. J. et al., 1998, Nature, 395, 670
Goldoni P., Royer F., François P., Horrobin M., Blanc G., Vernet J., Modigliani A., Larsen J., 2006, in McLean I. S., Iye M., eds, Proc. SPIE Conf., Vol. 6269, Ground-based and Airborne Instrumentation for Astronomy. p. 62692K
Gorosabel J. et al., 2003a, A&A, 400, 127
Gorosabel J. et al., 2003b, A&A, 409, 123
Graham J. F., Fruchter A. S., 2013, ApJ, 774, 119
Greiner J. et al., 2011, A&A, 526, A30
Hatsukade B., Kohno K., Endo A., Nakanishi K., Ohta K., 2011, ApJ, 738, 33
Heger A., Fryer C. L., Woosley S. E., Langer N., Hartmann D. H., 2003, ApJ, 591, 288
Hjorth J., Bloom J. S., 2012, in Kouveliotou C., Wijers R. A. M. J., Woosley S., eds, Cambridge Astrophys. Ser. 51, Gamma-Ray Bursts. Cambridge Univ. Press, Cambridge, p. 169
Hunt L. K. et al., 2014, A&A, 565, A112
Ilbert O. et al., 2006, A&A, 457, 841
Jakobsson P., Hjorth J., Fynbo J. P. U., Watson D., Pedersen K., Björnsson G., Gorosabel J., 2004, ApJ, 617, L21
Japelj J. et al., 2015, A&A, 579, A74
Kann D. A., Klose S., Zeh A., 2006, ApJ, 641, 993
Kennicutt R. C., Jr, 1998, ARA&A, 36, 189
Kewley L. J., Dopita M. A., 2002, ApJS, 142, 35
Kewley L. J., Ellison S. L., 2008, ApJ, 681, 1183
Kistler M. D., Yuksel H., Hopkins A. M., 2013, preprint (arXiv:1305.1630)
Klose S. et al., 2000, ApJ, 545, 271
Kobulnicky H. A., Kewley L. J., 2004, ApJ, 617, 240 (KK04)
Krühler T. et al., 2011, A&A, 534, A108
Krühler T. et al., 2015, preprint (arXiv:1505.06743)
Le Floc'h E. et al., 2003, A&A, 400, 499
Levesque E. M., Kewley L. J., Berger E., Zahid H. J., 2010, AJ, 140, 1557
MacFadyen A. I., Woosley S. E., 1999, ApJ, 524, 262
McGaugh S. S., 1991, ApJ, 380, 140 (M91)
Maiolino R. et al., 2008, A&A, 488, 463
Mannucci F., Cresci G., Maiolino R., Marconi A., Gnerucci A., 2010, MNRAS, 408, 2115
Mannucci F., Salvaterra R., Campisi M. A., 2011, MNRAS, 414, 1263
Masetti N. et al., 2005, A&A, 438, 841
Melandri A. et al., 2012, MNRAS, 421, 1265
Michałowski M. J., Hjorth J., Castro Cerón J. M., Watson D., 2008, ApJ, 672, 817
Modigliani A. et al., 2010, in Proc. SPIE Conf. Ser.,Vol. 7737, p. 28
Nagao T., Maiolino R., Marconi A., 2006, A&A, 459, 85
Nakajima K., Ouchi M., 2014, MNRAS, 442, 900
Osterbrock D. E., Ferland G. J., 2006, in Osterbrock D. E., Ferland G. J., eds, Astrophysics of Gaseous Nebulae and Active Galactic Nuclei. Univ. Science Books, Sausalito, CA
Paczyński B., 1998, ApJ, 494, L45
Perley D. A. et al., 2009, AJ, 138, 1690
Perley D. A. et al., 2013, ApJ, 778, 128
Perley D. A. et al., 2015a, preprint (arXiv:1504.02482)
Perley D. A. et al., 2015b, ApJ, 801, 102
Perley D. A. et al., 2015c, preprint (arXiv:1504.02479)
Pilyugin L. S., Thuan T. X., 2005, ApJ, 631, 231 (P05)
Piro L. et al., 2002, ApJ, 577, 680
Pita S. et al., 2014, A&A, 565, A12
Price P. A. et al., 2002, ApJ, 573, 85
Salpeter E. E., 1955, ApJ, 121, 161
Salvaterra R. et al., 2012, ApJ, 749, 68
Sarazin M., Roddier F., 1990, A&A, 227, 294
Savaglio S., 2010, in Cunha K., Spite M., Barbuy B., eds, Proc. IAU Symp. 265, p. 139
Savaglio S., Glazebrook K., Le Borgne D., 2009, ApJ, 691, 182
Schady P. et al., 2014, A&A, 570, A52
Schlafly E. F., Finkbeiner D. P., 2011, ApJ, 737, 103
Storey P. J., Zeippen C. J., 2000, MNRAS, 312, 813
Svensson K. M., Levan A. J., Tanvir N. R., Fruchter A. S., Strolger L., 2010, MNRAS, 405, 57
Thöne C. C., de Ugarte Postigo A., Vreeswijk P., D'Avanzo P., Covino S., Fynbo J. P. U., Tanvir N., 2010, GRB Coordinates Network, 10971, 1
van der Horst A. J., Kouveliotou C., Gehrels N., Rol E., Wijers R. A. M. J., Cannizzo J. K., Racusin J., Burrows D. N., 2009, ApJ, 699, 1087
van Dokkum P. G., 2001, PASP, 113, 1420
Vergani S. D. et al., 2010, GRB Coordinates Network, 10495, 1
Vergani S. D. et al., 2014, preprint (arXiv:1409.7064)
Vernet J. et al., 2011, A&A, 536, A105
Woosley S. E., 1993, ApJ, 405, 273
Woosley S. E., Heger A., 2006, ApJ, 637, 914
Yoon S.-C., Woosley S. E., Langer N., 2010, ApJ, 725, 940
Zahid H. J., Kewley L. J., Bresolin F., 2011, ApJ, 730, 137
Zahid H. J., Geller M. J., Kewley L. J., Hwang H. S., Fabricant D. G., Kurtz M. J., 2013, ApJ, 771, L19

This paper has been typeset from a TEX/LATEX file prepared by the author.

Downloaded from http://mnras.oxfordjournals.org/ at CNR on December 9, 2015